

Structural Basis of Non-specific Lipid Binding in Maize Lipid-transfer Protein Complexes Revealed by High-resolution X-ray Crystallography

Gye Won Han¹, Jae Young Lee², Hyun Kyu Song², Changsoo Chang²
Kyeongsik Min², Jinho Moon², Dong Hae Shin², Mary L. Kopka¹
Michael R. Sawaya¹, Hanna S. Yuan^{1,3}, Thomas D. Kim²
Jungwoo Choe², Dori Lim², Hee Jung Moon² and Se Won Suh^{2*}

¹*Molecular Biology Institute
University of California at Los
Angeles, Los Angeles
CA 90095-1570, USA*

²*School of Chemistry and
Molecular Engineering College
of Natural Sciences Seoul
National University Seoul
151-742, Korea*

³*Institute of Molecular Biology
Academia Sinica, Taipei
Taiwan, 11529, Republic of
China*

Non-specific lipid-transfer proteins (nsLTPs) are involved in the movement of phospholipids, glycolipids, fatty acids, and steroids between membranes. Several structures of plant nsLTPs have been determined both by X-ray crystallography and nuclear magnetic resonance. However, the detailed structural basis of the non-specific binding of hydrophobic ligands by nsLTPs is still poorly understood. In order to gain a better understanding of the structural basis of the non-specific binding of hydrophobic ligands by nsLTPs and to investigate the plasticity of the fatty acid binding cavity in nsLTPs, seven high-resolution (between 1.3 Å and 1.9 Å) crystal structures have been determined. These depict the nsLTP from maize seedlings in complex with an array of fatty acids.

A detailed comparison of the structures of maize nsLTP in complex with various ligands reveals a new binding mode in an nsLTP-oleate complex which has not been seen before. Furthermore, in the caprate complex, the ligand binds to the protein cavity in two orientations with equal occupancy. The volume of the hydrophobic cavity in the nsLTP from maize shows some variation depending on the size of the bound ligands.

The structural plasticity of the ligand binding cavity and the predominant involvement of non-specific van der Waals interactions with the hydrophobic tail of the ligands provide a structural explanation for the non-specificity of maize nsLTP. The hydrophobic cavity accommodates various ligands from C10 to C18. The C18:1 ricinoleate with its hydroxyl group hydrogen bonding to Ala68 possibly mimics cutin monomer binding which is of biological importance. Some of the myristate binding sites in human serum albumin resemble the maize nsLTP, implying the importance of a helical bundle in accommodating the non-specific binding of fatty acids.

© 2001 Academic Press

*Corresponding author

Keywords: non-specific lipid-transfer protein; fatty acid binding; hydrophobic cavity; antifungal activity; structural plasticity

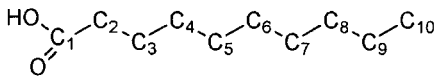
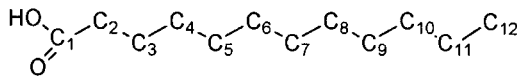
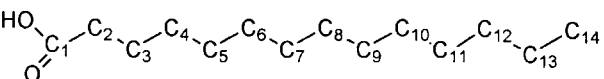
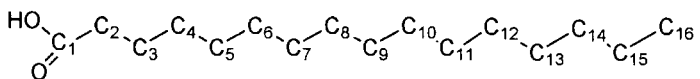
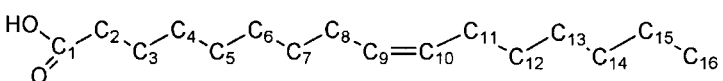
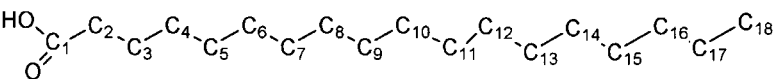
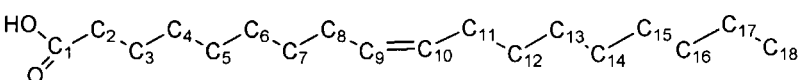
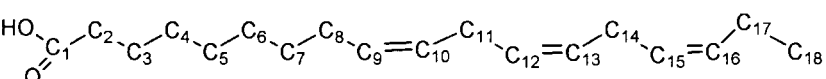
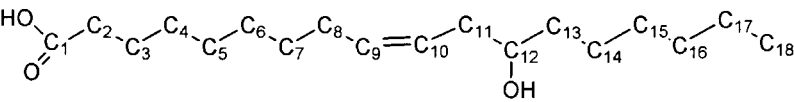
Abbreviations used: BPI, bactericidal/permeability-increasing protein; HPS, hydrophobic protein from soybean; HSA, human serum albumin; LMPC, lysomyristoyl-phosphatidylcholine; LTP, lipid-transfer protein; NMR, nuclear magnetic resonance; nsLTP, non-specific lipid-transfer protein; r.m.s., room-mean-square.

E-mail address of the corresponding author:
sewonsuh@snu.ac.kr

Introduction

Lipid-transfer proteins (LTPs) facilitate the transfer of lipids between membranes. They have been isolated from a diverse range of organisms, from bacteria and yeast to higher plants and animals.¹ Some LTPs are specific, whereas others are non-specific, exhibiting an affinity for a broad range of polar lipids. Despite sharing a lack of specificity, plant non-specific LTPs (nsLTPs) show no amino

Table 1. Schematic drawings of the ligands

Capric Acid C10:0	
Lauric Acid C12:0	
Myristic Acid C14:0	
Palmitic Acid C16:0	
Palmitoleic Acid C16:1, 9	
Stearic Acid C18:0	
Oleic Acid C18:1, 9	
Linolenic Acid C18:3, 9,12,15	
Ricinoleic Acid C18:1, 9,12-OH	

acid sequence similarity to mammalian LTPs. Plant nsLTPs are small (~9 kDa), disulfide-rich, basic proteins. A number of roles for plant nsLTPs have been proposed. They include the transfer of phospholipids from liposomes or microsomes to mitochondria,² the transport of cuticular components required for the biosynthesis of surface wax,³⁻⁵ and the inhibition of bacterial and fungal pathogens of plants.⁶⁻⁸ Furthermore, they bind fatty acids and acyl coenzyme A with high affinity and have been proposed to function as fatty acid and acyl coenzyme A carrier proteins.⁹⁻¹¹

Initially the tertiary structure of nsLTP from maize was predicted to be "all β -sheet".¹² However, an NMR study on wheat nsLTP in solution indicated that it is mainly α -helical.¹³ The solution structure of nsLTP from wheat¹⁴ and the crystal structure of nsLTP from maize¹⁵ revealed the first view of an nsLTP, showing a lack of β -strands and nearly two-thirds of the residues as α -helices. Since then, the crystal structure of nsLTP from rice¹⁶ as well as solution structures of nsLTPs from maize,¹⁷ barley,¹⁸ and rice¹⁹ have also been determined. In the absence of a bound ligand, these proteins have a tunnel-like hydrophobic cavity, which is large

enough to accommodate a long fatty acyl chain. All these structures share a common protein fold, first discovered in a hydrophobic protein from soybean (HPS).^{20,21} We propose that this kind of protein fold be called the “plant nsLTP fold”.

The crystal structures of maize nsLTP in complex with palmitate¹⁵ and wheat nsLTP with lyso-myristoyl-phosphatidylcholine (LMPC) at 2.1 Å resolution have been reported.²² They showed that the hydrocarbon tail of the ligand is inserted into the protein cavity and the head group is exposed on the protein surface. Unfortunately, the choline head group of LMPC was not resolved in the electron density map due to high *B*-factors. Solution structures of barley nsLTP complexed with palmitate²³ and with palmitoyl coenzyme A,¹⁸ maize nsLTP complexed with 1-palmitoyl-2-lysophosphatidylcholine,¹ and wheat nsLTP complexed with 1,2-dimyristoylphosphatidylglycerol²⁴ have also been reported. In these structures, the hydrocarbon tails of the fatty acids are also inserted into the protein cavity. However, the solution structure differs from the crystal structure in that the ligands are inserted from the opposite end of the tunnel-like hydrophobic cavity. This suggests that two orientations are possible for hydrophobic ligands to bind to plant nsLTPs.²³ Furthermore, the recent solution structure of nsLTP(wheat):prostaglandin B₂ complex²⁵ shows that the ligand was fully embedded in the hydrophobic core of the protein.

In order to improve our understanding of how hydrophobic ligands of different length and shape are accommodated in the binding cavity of nsLTPs it is necessary to perform a more systematic study of protein ligand interactions with a series of fatty acids (see Table 1). Here we have determined a number of high-resolution crystal structures of maize nsLTP in complex with an array of hydrophobic ligands, saturated or unsaturated fatty acids, ranging in size from C10 to C18. These structures allow us to determine precisely ligand-protein interactions and to examine how the hydrophobic cavity of maize nsLTP accommodates different hydrophobic ligands for non-specific binding. Furthermore, we have compared the crystal structures of maize nsLTP with proteins having similar binding modes, such as human serum albumin (HSA).

Results and Discussion

Overall structure and quality of the models

The structures of the maize nsLTP in complexes with various fatty acids (Table 1) at 1.8-1.9 Å or 1.3 Å resolution have been refined with crystallographic *R*-factors of 17.1-21.4% (*R*_{free} of 17.7-27.4%) and the root-mean-square (r.m.s.) deviation from the ideality is 0.009-0.016 Å and 1.60-2.20° for bond lengths and bond angles, respectively. As in the uncomplexed structure, the final models of maize nsLTP complexes fold into a single compact

domain consisting of four α -helices and a long C-terminal loop region, with four disulfide bonds interconnecting the secondary structure elements (Figure 1). The tunnel-like hydrophobic cavity is occupied by the hydrophobic tail of the ligand in the complexed models.

The overall r.m.s. differences between complexed and uncomplexed structures are in the range 0.79-0.94 Å. The major differences between complexed and uncomplexed structures are localized in the C-terminal loop region. The overall

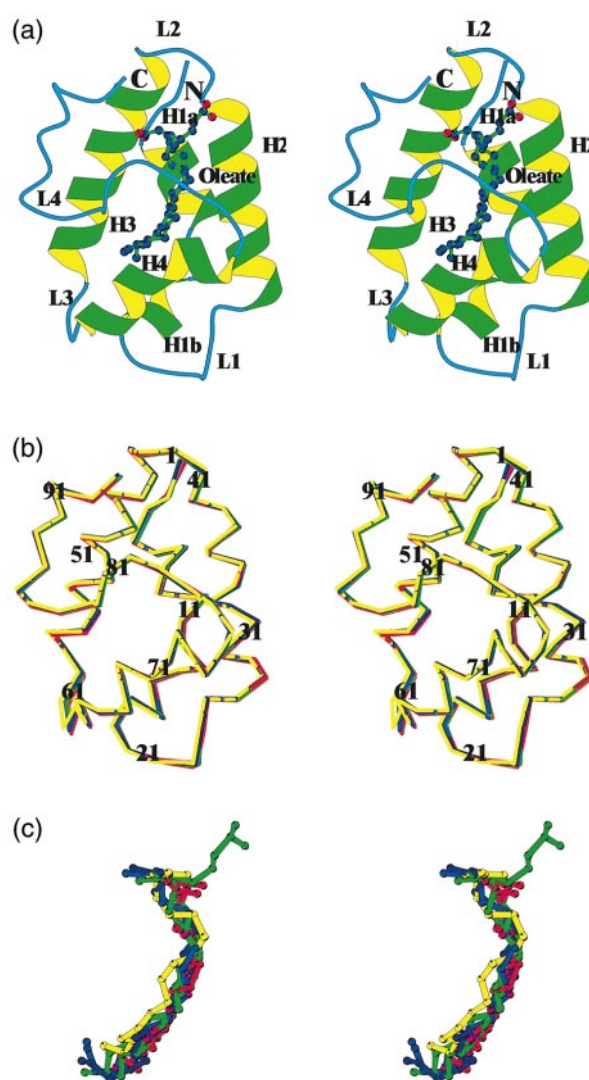


Figure 1. (a) Stereo ribbon diagram of maize non-specific lipid-transfer protein complexed with oleate. The Figures were drawn with the MOLSCRIPT program.⁴¹ (b) Superposition of the backbone trace of eight nsLTP complexes. (c) Bound fatty acids showing structural comparisons between complexes. Colors used in (b) and (c): nsLTP:caprate (purple), nsLTP:laurate (red), nsLTP:myristate (dark red), nsLTP:palmitoleate (green), nsLTP:stearate (blue), nsLTP:oleate (dark green), nsLTP:linoleate (yellow), and nsLTP:ricinoleate (dark blue).

average B -factors of complexed structures are in the range 12.4-22.7 \AA^2 .

Figure 2(a) shows molecular surfaces colored by B -factors. Only two complexes, C10 caprate and C18 ricinoleate, are shown here. The remaining nsLTP fatty acid complexes showed similar pat-

terns. Among the complexes, one can notice a similar pattern of B -factor distribution. However, the B -factor distribution of uncomplexed nsLTP is slightly different (note the blue region around the cavity, which changes to red on complexation). The B -factors around the cavity of complexed

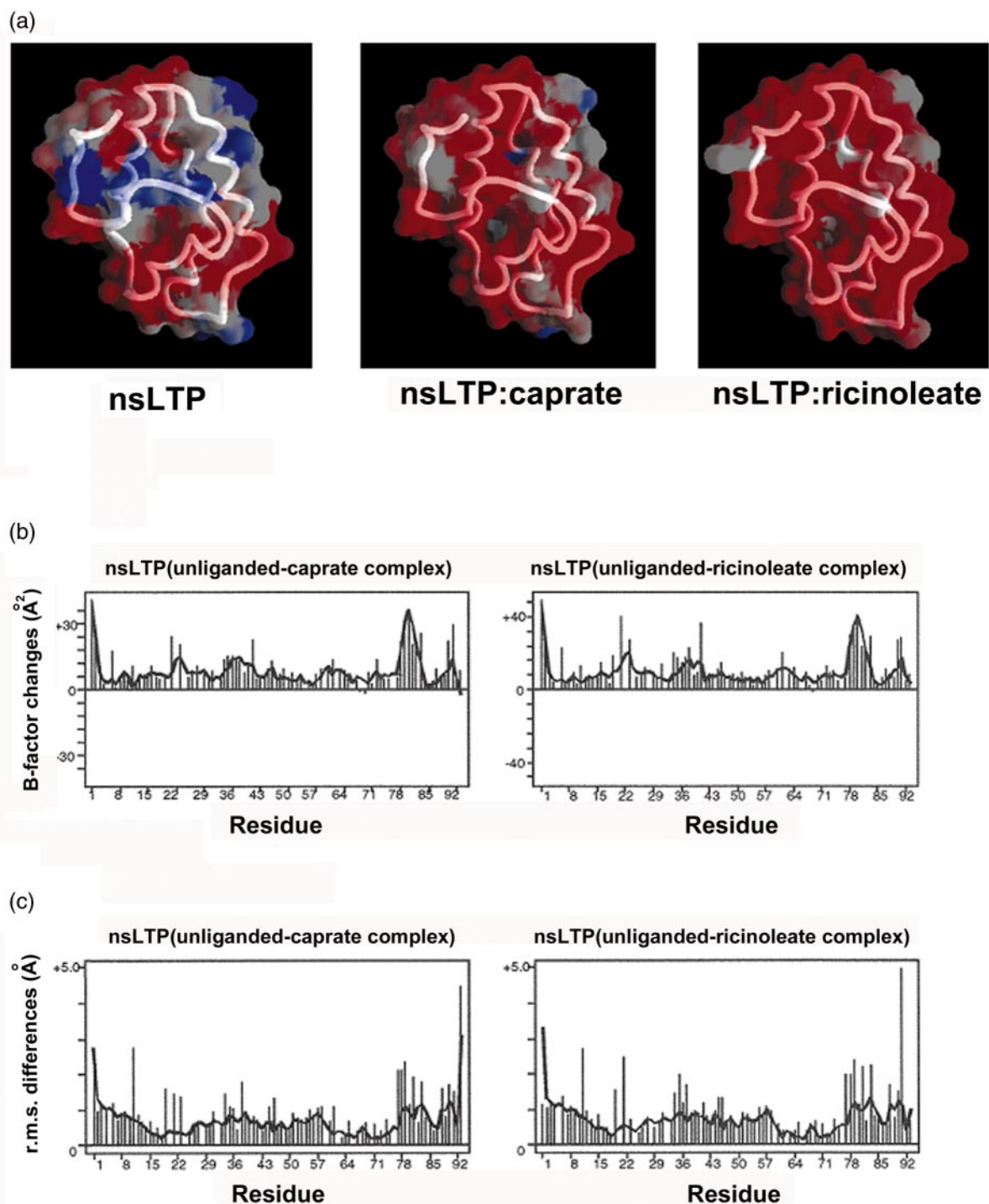


Figure 2. (a) The comparison of B -factors of molecular surfaces calculated for uncomplexed and complexed nsLTPs with the ligand omitted for clarity. The surface color from blue to red represents β -factors from 59.29 to 14.6 \AA^2 . The GRASP program⁴² was used to display B -factors for (a). (b)-(c) The comparison of r.m.s. differences between uncomplexed and complexed nsLTPs. Main-chain atoms (continuous lines) and side-chain atoms (continuous rods) of each residue are plotted in (b) and (c).

structures (residues Ile11, Ser14, Ile15 and Ala18 in helix H1; Val33 and Leu36 in helix H2; Ala40 of loop L2; Ala49, Leu53, Ala56, Ala57 of helix H3; Val60 and Leu63 of loop L3; Ala68, Ile71 and Pro72 of helix H4 and Val77, Ile79 and Ile83 in the C-terminal region) are decreased by $\sim 25 \text{ \AA}^2$ (Figure 2(a)). Figure 2(b) shows *B*-factor differences between uncomplexed protein and the complexes for caprate and ricinoleate. The largest difference is observed at residues 78-81, near the C-terminal loop. These regions correspond to regions of the highest r.m.s. deviation in superimposed atomic coordinates. (Figure 2(c)).

Structural plasticity of the hydrophobic cavity

One of the most prominent features in the crystal structure of maize nsLTP is the presence of a hydrophobic cavity, which runs through the protein (Figure 3). It is tunnel-like, resembling a curved, hollow tube with an opening (termed the "top" opening) at one end near the C terminus of helix H2, another opening (termed the "bottom" opening) at the opposite end near the C terminus of helix H3, and a small fracture on the side between helix H4 and a part of the C-terminal loop region. The side gap is filled with ordered water molecules (see Figure 7(a) of ref. 15). The head groups of the bound ligands are stretched out, contacting the surface residues and water molecules. However, the hydrophobic tails of bound ligands are buried inside the hydrophobic cavity (Figure 3). The van der Waals volume of the hydrophobic cavity shows a dependence on the size of the bound ligand, varying between 547 and 620 \AA^3 . The van der Waals volume of the hydrophobic cavity in the uncomplexed nsLTP is 399 \AA^3 , calculated by VOIDOO²⁶. This value is slightly different from that calculated by GRASP, 408 \AA^3 , which we used previously.¹⁶ So we recalculated the volume for all the complexes using the VOIDOO program to make an accurate comparison. The cavity volume increases slightly as the length of the bound fatty acid increases from C10 to C16: caprate, 558 \AA^3 ; laurate, 547 \AA^3 ; myristate, 566 \AA^3 ; palmitate, 582 \AA^3 ; palmitoleate, 569 \AA^3 . It also shows some dependence on the shape of C18 saturated and unsaturated fatty acids: stearate, 557 \AA^3 ; oleate, 564 \AA^3 ; ricinoleate, 620 \AA^3 ; linolenate, 605 \AA^3 . A similar trend was observed in the probe-accessible cavity volumes that are calculated by measuring the volume occupied by the centers of probe atoms using a radius of 1.4 \AA as the probe moves through the cavity. They are caprate, 110 \AA^3 ; laurate, 122 \AA^3 ; myristate, 134 \AA^3 ; palmitate, 138 \AA^3 ; and palmitoleate, 133 \AA^3 . For C18 fatty acids, they are stearate, 124 \AA^3 ; oleate, 128 \AA^3 ; ricinoleate, 146 \AA^3 ; and linoeneate, 146 \AA^3 . The ligand-dependent variation of the cavity volume implies a structural plasticity of the hydrophobic cavity, that is, the cavity of maize nsLTP can swell or contract to a certain extent to accommodate a variety of bound ligands. This plasticity may be due to the

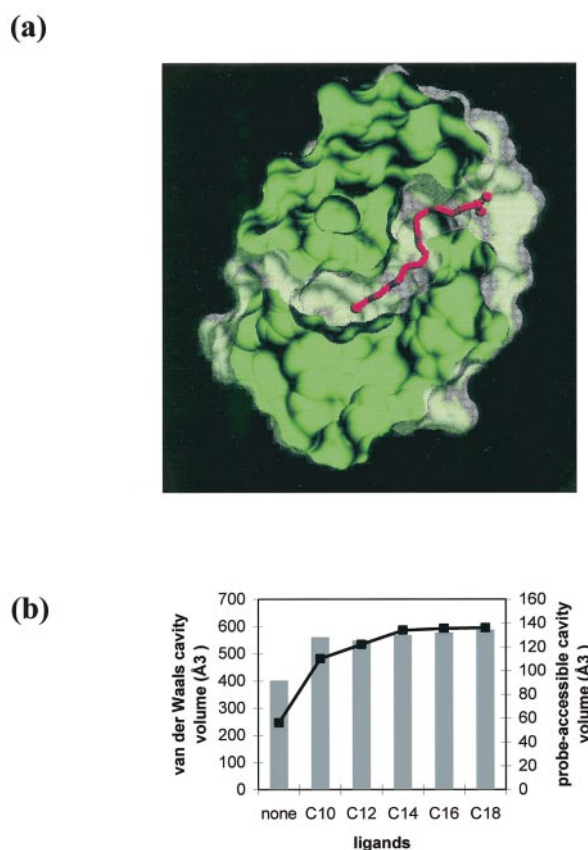


Figure 3. (a) The oleate model in the hydrophobic cavity (drawn with MSP⁴³). (b) Fatty acid-binding-induced volume changes in nsLTP complexes. For all calculations, the fatty acid has been removed from the cavity. Rods show the van der Waals volumes of hydrophobic cavities and a line shows the volume of the probe-accessible cavity using a probe radius of 1.4 \AA .

predominance of aliphatic residues lining the cavity.¹⁵ Figure 3(b) shows fatty acid-binding-induced volume changes. For the complexes, the van der Waals cavity volume is larger than that of the uncomplexed protein, but within the complexes, it remains constant. However, the probe-accessible cavity volume, also calculated by VOIDOO, indicates more of a dependence on the size of bound ligands; the cavity size increases somewhat with acyl chain length from C12 to C16, with almost no change from C16 to C18. The average cavity volume of the complex of C18 ligands is 136 \AA^3 , which is almost the same as that of the C16 complexes. This implies that the optimal cavity volume for nsLTP is for ligands between C16 and C18. Among C18 ligands, the volume of the probe-accessible surface of stearate and oleate is similar to C16 palmitate and palmitoleate complexes. However, linolenate has a bigger probe-accessible

Table 2. Torsion angles, *B*-factors and van der Waals contacts (within 4.5 Å) of bound fatty acids

Carbon atom	Torsion angles (°)	<i>B</i> -factor (Å ²)	Contacts	Carbon atom	Torsion angles (°)	<i>B</i> -factor (Å ²)	Contacts
Caprate				Palmitoleate			
C1	-163	47.1	V33, N37, L53, I79	C1	164	39.1	R46, I79, Y81
C2	179	44.2	V33, L36, L53	C2	-136	38.2	N37, A40, R46
C3	-148	39.5	V33, L53, I83	C3	79	37.1	A40, A49, L53
C4	149	35.2	V33, I83	C4	-179	37.3	L36, N37, L53
C5	-177	32.7	V33, P72, I83, sol180	C5	-96	38.0	L53, I79
C6	178	30.9	I11, V33, L53, I71, I83	C6	-62	38.8	V33, N37
C7	-121	31.2	I71, I83, sol180	C7	-107	40.5	V33, L36, L53
C8	-165	34.9	I71, sol180	C8	-99	41.6	V33, L53
C9		36.0	I11	C9	0	43.6	V33, P72
C10		38.0	I11, I15, A18, V60	C10	-135	44.9	V33, I71, P72
Laurate				C11	-99	46.2	I11, V33, L53
C1	76	41.3	N37, I79, sol143, sol152, sol168	C12	-132	47.8	I11, L53, sol513
C2	-97	35.3	L36, A40, A49, L53, sol143	C13	-126	49.8	I11, C14, I71, sol513
C3	-179	33.0	L36, L53, I79, sol143	C14	63	51.1	I11, C14, I15, sol513
C4	79	28.1	V33, L36, N37, I79	C15		51.6	C14, I15, A18, sol513, I71
C5	-161	29.0	V33, I79	C16		52.5	A18, A68, I71, sol513
C6	-164	28.5	V33, L36, L53, I83	Stearate			
C7	-157	28.6	V33, P72, I83	C1	101	39.0	R46, Y81, sol5, sol144, sol147
C8	-177	29.5	I11, V33, L53, I71, I83	C2	-142	36.1	A40, R46, A49, Y81, sol147
C9	-115	30.4	I71, I83	C3	-171	34.5	A49, L53, I79, Y81, sol147
C10	175	32.0	I71	C4	-110	31.6	N37, L53, I79, sol147
C11		33.6	I11	C5	132	32.5	L36, N37, L53
C12		35.3	I11, I15	C6	76	32.3	V33, N37, I79
Myristate				C7	-176	35.1	V33, I79, I83
C1	101.7	23.2	A40, N37, R6, I79, sol318, sol254, sol277	C8	174	35.5	V33, I83
C2	-73	25.6	L36, A40, A49, N37, R46, sol277	C9	-139	38.6	V33, P72, I83, sol2
C3	-162	21.9	L36, A49, L53, sol277	C10	148	41.1	V33, I71, I83, sol2
C4	-142	23.3	L36, N37, I79	C11	123	44.9	L53, I83, sol2, sol198
C5	156	25.6	L36, V33, N37	C12	-173	47.5	I11, L53, sol2
C6	-14	25.7	V33, N37, V77	C13	-125	50.0	I71, sol2
C7	119	26.0	V33, P72, V77, I79	C14	6	53.0	I11, C14, I15, sol2
C8	109	23.7	V33, L53, P72, I79	C15	72	53.9	I15, A18, V60
C9	137	21.8	I11, V33, L53	C16	-133	55.2	A18, A56, A57, V60
C10	-129	19.1	V33, I71	C17		56.2	L53, A56, A57
C11	-169	22.3	I11, L53, I71	C18		56.5	L53, A57, I83, sol198
C12	21	27.4					
C13		30.7					
C14		35.3	I11, C14, A18, I71				

surface volume, 146 Å³. It seems that linolenate with three *cis*-double bonds needs a larger space.

Ligand-protein interactions and the structural basis of non-specific binding

Accurate models of bound ligands are a prerequisite for the analysis of ligand-protein interactions. In order to avoid any bias from the previously built models of the complexes, the bound ligand in each complex structure was independently modeled into the electron density. Most

of the ligands have been defined by continuous electron density of sufficient length and their models could be built in one conformation. In all cases except for caprate and oleate, the orientations of the bound ligands were clearly discernible due to the bulky electron density for the head groups and their orientations are the same as in the previously reported crystal structure of the maize nsLTP:palmitate complex.¹⁵ Contacts for all ligands are shown in Table 2.

For the caprate complex, the electron density does not show the bifurcated shape of the carboxy-

Table 2. (continued).

Carbon atom	Torsion angles (°)	B-factor (Å ²)	Contacts	Carbon atom	Torsion angles (°)	B-factor (Å ²)	Contacts
Linolenate				Ricinoleate			
C1	-151	27.1	N37, R46, I79	C1	-175	21.3	R46, Y81, sol434, sol441
C2	-62	24.4	R46, W81	C2	180	23.3	A40, R46, A49, Y81, sol441
C3	119	25.8	R46, W81	C3	-67	22.9	A49, L53, Y81, sol441
C4	19	24.1	A40, R46, A49, W81	C4	155	23.7	L36, A40, A49, L53
C5	-167	25.7	L36, A40, A49	C5	-126	24.1	L36, N37
C6	-145	26.2	L53	C6	159	22.7	V33, L36, N37, L53
C7	-77	27.8	L36, N37, L53	C7	-139	22.7	V33, L53, I79
C8	-176	25.2	L36, L53	C8	161	21.8	V33, sol464
C9	-6	26.1	L53	C9	24	21.9	V33, L53, sol464
C10	-173	29.1	V33, L53, P72, I79	C10	-164	23.2	L53, I83, sol464
C11	114	25.9	V33, L53	C11	-161	24.0	V33, I71, sol464
C12	33	27.9	V33, I71, P72	C12	-143	26.4	A68, I71, sol464
C13	89	26.3	I71, sol152	O12		29.4	A68, I71, P72, I83, sol44, sol445, sol464
C14	94	28.4	L53	C13	178	28.9	A57
C15	54	29.5	I11, L53, sol201	C14	-157	31.1	A57, I83
C16	-178	29.8	I71, sol201	C15	-175	30.8	A57
C17		27.2	A57, sol201	C16	-174	32.7	A18, A68, I71
C18		26.4	A18, A56, A57, V60, sol201	C17		32.8	I11, C14, I15, A18, I71
				C18		37.7	I11, C14, I15
Oleate (conformation 1)				Oleate (conformation 2)			
C1	-175	36.56	N37, sol 457, sol564, A40, R46, sol360, sol361, sol383, sol665	C1	101	41.95	R46, C50, Y81, R46, V92, sol351
C2	-168	37.56	N37, sol564, A40, R46, sol 360, sol361, sol383, sol 665	C2	26	40.19	R46, Y81, sol383, sol351
C3	106	37.40	N37, A40, R46, sol360, sol383, sol665	C3	38	41.00	N37, R46, I79, sol360, sol383
C4	82	39.58	N37, R46, I79, sol360, sol383	C4	116	39.05	N37, A40, I79, sol383
C5	84	39.37	N37, R46, I79, sol351, sol383	C5	114	39.15	L53, A40, A49
C6	-158	39.27	A40, R46, A49	C6	-77	39.07	L36, N37, A40
C7	95	38.24	L53, Y81, I79	C7	36	39.22	L36, V33, N37, L53
C8	107	38.53	L36, L53	C8	125	39.60	V33, L36, N37
C9	11	39.73	V33, N37, I79	C9	-7	40.20	V33, I79
C10	174	39.93	V33, V77, I79	C10	123	40.41	V33, I79, I83
C11	-134	40.52	V33, L53, I79, I83	C11	135	40.64	V33, L53, I83
C12	-146	40.82	V33, P72, I83	C12	165	41.41	V33, I71, I83
C13	-179	41.06	V33, L53, I83	C13	-170	41.94	V33, I71, I83
C14	-162	42.06	I71, P72, I83, sol359	C14	130	42.29	V33, I71
C15	147	42.48	L53, I83	C15	159	42.78	I71, sol359
C16	120	43.34	I71, A68, sol359	C16	179	43.62	I11
C17		43.15	Sol359, sol1160	C17		43.67	A57, sol359
C18		41.92	I71, A18	C18		41.43	I15, V60, A57, A56, A18

late moiety and X-ray diffraction data alone cannot distinguish the two possible orientations, caprylate tail up or down (Figure 4(a)). The values of R -factor (R_{free}) of the two models are 0.2145 (0.2416) and 0.2141 (0.2419), respectively. Both modes of caprate chains are straight, having $\sim 180^\circ$ torsion angles and van der Waals interactions with Val33, Leu36, Ile71 and Ile83 (Table 2). With two conformations of caprate with half occupancy for each, the R -factor and R_{free} are 0.201 and 0.231, respectively (Figure 4(b)). It is likely that caprate binds to the cavity in both orientations. The inverted mode of

binding (B in Figure 4(b)) was observed in the solution structures of barley nsLTP in complex with palmitate²³ and palmitoyl coenzyme A.¹⁸ For caprate, which contains all single bonds in its C10 hydrocarbon tail, there are no strong interactions with the residues of the interior wall of the cavity. There is no hydrogen bond between the oxygen atoms of the carboxylate group of caprate and atoms from the residues Tyr81, Arg46, and Asn37. This may explain why caprate binds in both orientations. In this complex, the side-chains of Tyr81 and Asn37 are involved in the hydrogen-bond net-

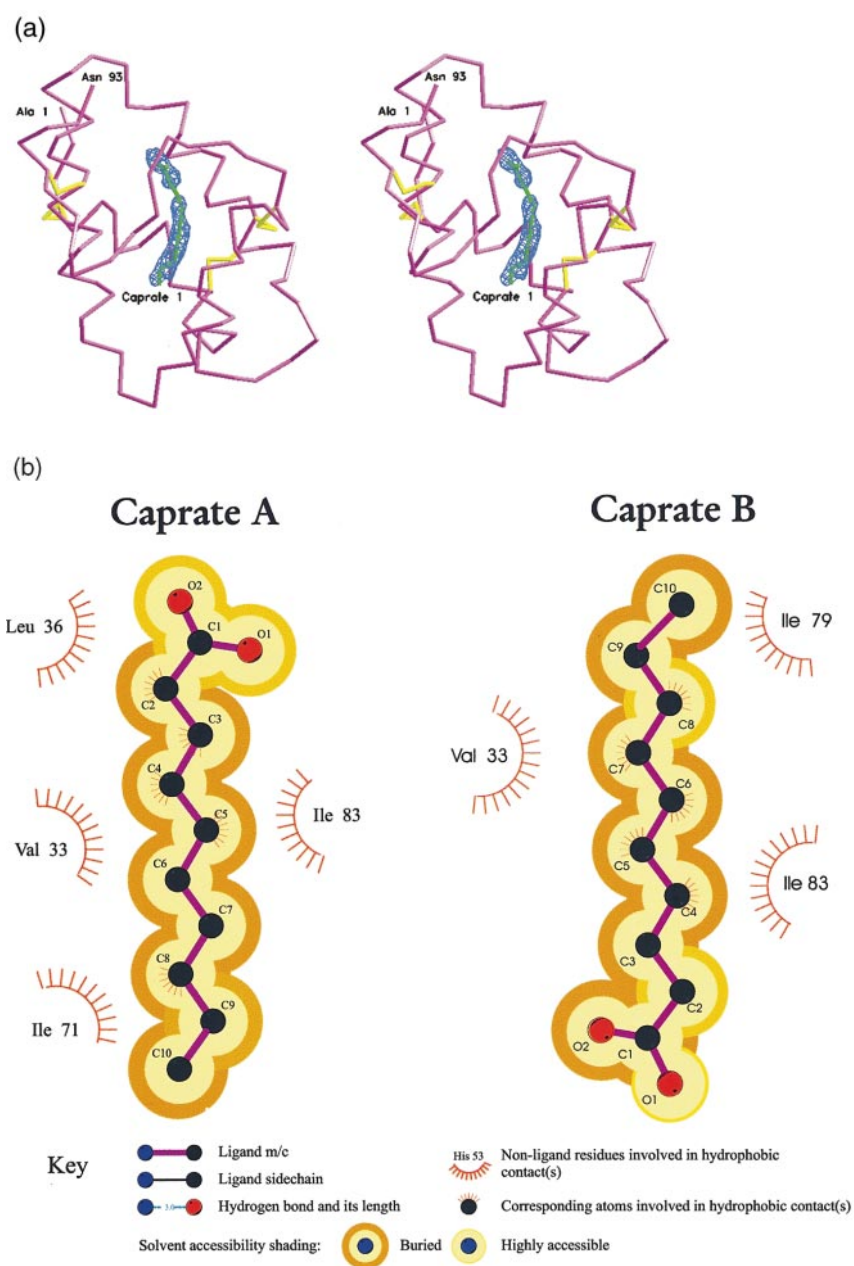


Figure 4. (a) Stereoview of a $F_o - F_c$ omit electron density map of nsLTP:caprate showing binding mode 1. The map was contoured at the 2.7σ level. The coordinates of this region were omitted and the protein coordinates were refined by X-PLOR³⁵ before the phase calculation. (b) A representation of the two different caprate-binding interactions is shown by LIGPLOT.

work with water molecules 401 and 402 instead. The average B -factor of capric acid is 33.4 \AA^2 (Table 2).

Unlike C12 laurate and C14 myristate, which contain hydrogen bonds with the side-chain of Asn37, the carboxylate head groups of the longer C16 fatty acids, palmitate and palmitoleate, are hydrogen bonded with the OH group of Tyr81. In the nsLTP:laurate complex, the hydrocarbon tail of laurate contains all single bonds, the O1 carboxylate atom of laurate is hydrogen bonded with ND2 of Asn37 with a distance of 2.96 \AA . The other oxy-

gen, the O2 atom of the carboxylate group, is very weakly hydrogen bonded with water molecules 152 and 168 with distances of 3.60 and 3.53 \AA , respectively. For myristate, which contains all single bonds in the C14 hydrocarbon tail, the binding interaction is similar to that of nsLTP:laurate. The O1 atom of myristic acid is hydrogen bonded with ND2 of Asn37 and water 318. The O2 atom of myristic acid is hydrogen bonded with water molecules 254 and 277 with distances of 2.95 and 2.77 \AA , respectively.

Palmitoleate and palmitate C16 fatty acids, due to their length, have a different binding mode than laurate and myristate. The head group of palmitoleate is stretched out in the place formerly occupied by water molecules in nsLTP:caprate, nsLTP:laurate, and nsLTP:myristate. The binding modes of palmitate and palmitoleate are very similar. The O1 atoms of the palmitate and palmitoleate's carboxylate groups participate in hydrogen bonds with the OH group of Tyr81. The O2 atom of palmitoleate's carboxylate group is hydrogen bonded with the OH of Tyr81 with a distance of 3.15 Å. The difference is 2.86 Å between the O2 atom of palmitate's carboxylate group and the OH group of Tyr81.

Still larger fatty acids can be accommodated by nsLTP by maintaining hydrogen bonding with Tyr81, and by participating in different hydrogen-bonding networks. Various C18 fatty acids from nsLTP:stearate, nsLTP:oleate, nsLTP:ricinoleate, and nsLTP:linoleate show different binding interactions from each other.

In the nsLTP:stearate complex, the stearate consists of all single bonds in its C18 hydrocarbon chain. The O2 atom of stearate is hydrogen bonded with the OH of Tyr81 with a distance of 2.55 Å. The O1 carboxylate atom of stearate is hydrogen bonded with water molecules 144 and 205 with distances of 3.15 and 2.83 Å, respectively.

For oleate (C18:1, 9), the $F_o - F_c$ electron density also suggests two different conformations for binding (Figure 5(a)). The hydrocarbon tail of oleate contains all single bonds except the C9=C10 double bond. One conformation of the carboxylate group is bound in the usual location, the other conformation is new. Each model gives essentially identical values of R -factor (R_{free}) when two independent refinements were carried out.

The interactions of oleate of conformation 1 (Figure 5(a)) involve hydrogen bonds with two additional water molecules, because the head group of oleate is more exposed at the protein surface in conformation 1. The O1 atom of the oleate conformation 1 is hydrogen bonded with water 361 and the NH2 group of Arg46 with distances of 2.75 Å and 3.01 Å, respectively (Figure 5(b)). The O2 atom of oleate is hydrogen bonded with water molecules 564 and 665 with a distance of 3.19 Å and 3.05 Å, respectively. The O2 atom also donates the proton to either oxygen atom of Asn40 or Ala37 (not shown in Figure 5(b)). The distance between the O2 and oxygen backbone of Asn40 and Ala37 is 2.67 and 3.14 Å, respectively.

In conformation 2 of oleate (the usual conformation), the O1 atom of the carboxylate group is hydrogen bonded with the OH of Tyr81 and water 351 with distances of 2.65 Å and 3.03 Å, respectively. The O2 atom of oleate makes a hydrogen bond with the OH group of Tyr81 with a distance of 2.72 Å and the oxygen atom of Arg46 could be hydrogen bonded with O2 atom also (Figure 5(b)).

In the linoleate complex, the O2 atom of linoleate is hydrogen bonded with the OH of Tyr81

and water 223 with distances of 2.77 and 3.02 Å, respectively.

For ricinoleate in nsLTP:ricinoleate, the C18 hydrocarbon chain is the same as oleate except for the addition of one OH group at C12. The O1 atom of the carboxylate group of nsLTP:ricinoleate is hydrogen bonded with the OH of Tyr81 and water molecules 441 and 434 with distances of 2.78, 3.50, and 2.92 Å, respectively. The O2 atom of the carboxylate group is hydrogen bonded with water 434 with a distance of 3.27 Å. The hydroxyl group of C12 is hydrogen bonded with the oxygen atom of Ala68, and water molecules 444 and 464 with distances of 3.38, 3.09, and 3.19 Å, respectively.

Most of the hydrocarbon chains of the bound fatty acids are bent to fit into the curved tunnel-like cavity of nsLTP except C10 caprate, which is the shortest ligand. The torsion angles in Table 2 show that the bending modes of each fatty acid are different due to the different length and shape of these ligands.

In most of the nsLTP complexes, except for caprate and oleate as mentioned above, one of the two possible orientations of the fatty acids is predominantly favored due to the interactions with Tyr81, Arg46, and Asn37. These three residues, all located along the top opening of the cavity, as well as several ordered water molecules, are responsible for interaction with the carboxylate group of most of the bound ligands. Tyr81 and Arg46 are strongly conserved among plant nsLTPs, while Asn37 is replaced by Lys or His in other nsLTPs.¹⁶

The detailed ligand-protein interactions are significantly different from one ligand to another, depending on the length of hydrocarbon tail of each fatty acid. The hydroxyl group at carbon 12 of ricinoleate (18:1) is hydrogen bonded to Ala68, which is strongly conserved among plant nsLTPs.¹⁶ This suggests that one of the physiological ligands for plant nsLTPs may be hydroxyl fatty acids such as cutin monomers. Cutin is formed from 16:0 and 18:1 fatty acids with hydroxyl or epoxide groups. Although the presence of a hydrogen bond in this ricinoleate complex with a distance of 3.69 Å is not a strong binding interaction, it may be important in transporting cutin monomers during the formation of the cutin layer. However, other ligands can also be accommodated in the cavity with van der Waals contacts only, therefore, maintaining nsLTP's non-specific binding properties of transporting various fatty acids between membranes.

The structural plasticity of the ligand binding cavity and the involvement of van der Waals interactions only between the cavity and the hydrophobic ligands provide a structural basis for explaining the non-specificity of maize nsLTP.

Comparisons with other nsLTPs and functionally related proteins

Maize nsLTP shows the highest level (79%) of sequence identity with rice nsLTP and the two structures show r.m.s. deviation of 1.2 Å for 91

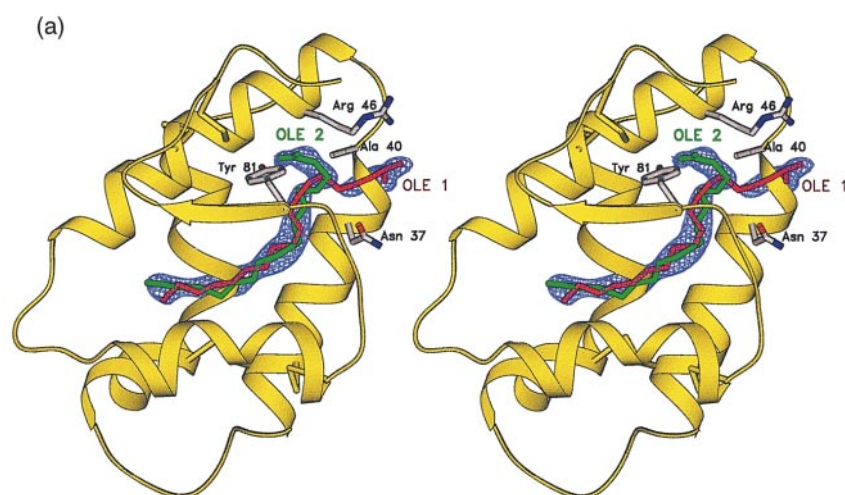


Figure 5 (legend opposite)

common C α atoms.¹⁶ However, the van der Waals volume of the hydrophobic cavity in rice nsLTP is much smaller than that of maize nsLTP;¹⁶ the difference is ~ 260 Å³. Until now it has not been possible to obtain crystals of rice nsLTP complexed with hydrophobic ligands. Therefore our comparison of the complexed structures is limited to nsLTP from barley, for which the sequence identity with maize nsLTP is 54%. The two structures that are compared are the crystal structure of nsLTP(maize):palmitate complex (PDB code: 1mzm) and the NMR structure of nsLTP(barley):palmitate complex (PDB code: 1be2). The solution structures of the nsLTP(barley):palmitate complex were averaged for comparison. When the amino acid sequences of nsLTPs from maize and barley are compared, the maize sequence indicates two insertions (Ala1 and Gln21). The insertion of Gln21 occurs in the loop L1 between the two α -helices H1 and H2. Among 43 residues identical between maize and barley nsLTPs, most of them are located on the protein surface, except the seven (Ile11, Ile15, Ala18, Asn37, Ala50, Val60, and Ile79 in maize) that are buried. The overall structure of nsLTP(barley):palmitate is very similar to that of nsLTP(maize):palmitate. A superposition gives an overall r.m.s. deviation of 2.25 Å for 91 common C α atoms. The comparison of the C α r.m.s. distances between maize and barley nsLTPs as a function of residue number shows large differences in two regions. One of them is the region where the insertion of Gln21 of the maize sequence occurs. This one-residue insertion results in a large displacement (over 4.0 Å) of residues 22–24 with an r.m.s. deviation of 4.84 Å for their C α atoms. Another region showing a large structural difference is the C-terminal segment between residues 80 and 81, with an r.m.s. deviation of 4.40 Å for two C α atoms.

In the fatty acid complex structures of maize nsLTP, most of the acyl chains are buried inside

the hydrophobic cavity, but the carboxylate group is exposed. The flexibility of the side-chains lining the hydrophobic cavity is the major contributor to the structural plasticity of the cavity. This plasticity allows a wide variety of ligands to bind in the cavity. Two residues, Arg46 and Tyr81, located strategically near one entrance to the hydrophobic cavity, can possibly interact with the polar head of the bound hydrophobic ligands. A comparison of liganded structures of maize nsLTP with the unliganded structure of rice nsLTP illuminates plausible roles of Arg46 and Tyr81. Tyr81 of liganded maize nsLTP protrudes out of the cavity slightly more in the unliganded state, allowing the OH group of Tyr81 to contact the carboxylate group of fatty acids when bound. The uncomplexed structure of rice nsLTP shows that Tyr79 (corresponding to Tyr81 in maize) is collapsed into the cavity, making its cavity considerably smaller than that of maize nsLTP.¹⁶ This probably explains why it is more difficult to grow crystals of rice nsLTP in complex with hydrophobic ligands. The side-chain of Arg44 in rice nsLTP swings down toward the hydrophobic cavity and blocks the entrance to the fatty acid binding cavity. However, the corresponding residue (Arg46) of maize nsLTP is stretched out toward the bulk solvent. It may also play an important role in the opening and closing of the entrance to the hydrophobic cavity for fatty acid binding. Since the hydrophobic tunnel in maize and barley nsLTPs is large enough to accommodate only a single acyl chain, the other chain of a phospholipid would have to be exposed to the solvent. In the nsLTP(maize):phosphatidylcholine complex, we propose that Arg46 would contribute to holding the head group of phosphatidylcholine and that Arg46 and Tyr81 may be critical for the phospholipid-transfer at the membrane.

In the wheat nsLTP:LMPC complex, there are two lipids inserted head to tail from opposite ends of the hydrophobic cavity.²⁵ Thus, the hydrophobic

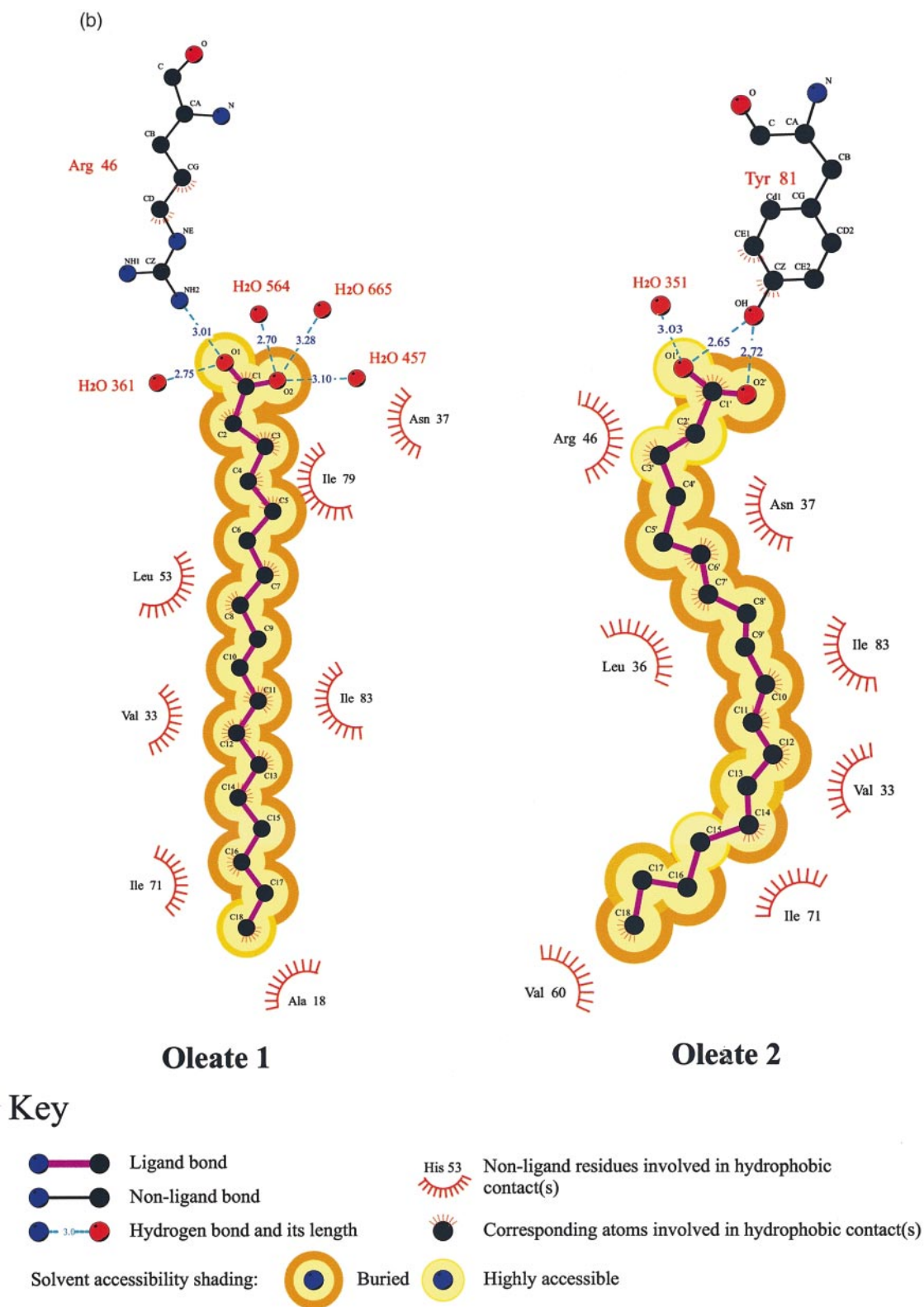


Figure 5. (a) Stereoview of a $F_o - F_c$ omit electron density map of nsLTP:oleate showing two conformations for the carboxylate tail. The map was contoured at the 3σ level and displayed by using the SETOR program.⁴⁴ The coordinates of this region were omitted and the protein coordinates were refined by SHELXL-97³⁸ before the phase calculation. (b) A LIGPLOT representation of the two different oleate-binding interactions.

cavity is divided into site 1 and site 2. There are two distinct differences between the maize and wheat nsLTP cavities that explain why maize nsLTP binds only a single fatty acid. In maize, the side-chain of Ile83 blocks part of what would be called site 1 and Ile15 blocks part of what would be called site 2. It is impossible to insert two aliphatic chains in the cavity for this reason unless accompanied by a large conformational change. So far, we have no evidence of such conformational changes in any of our 1:1-1.5:1 (lipid: protein) structures. Perhaps with a higher lipid:protein ratio, such as that used in the wheat complex (4:1), a conformational change may occur and accommodate the binding of two acyl chains. Further experiments with a higher ratio of fatty acids may clarify this discrepancy.

The crystal structure of human serum albumin (HSA) in complex (PDB code: 1bj5) with five molecules of myristate has been determined.²⁷ The protein is largely α -helical and has an unusually large number of disulfide bonds. It has three repeating domains, I-III, each of which contains two sub-domains (A and B) that share common helical motifs. Each sub-domain of HSA is about the same size as plant nsLTPs. Despite the lack of any significant sequence similarity between HSA and plant nsLTPs, it appears that, at least for some of the myristate binding sites of HSA, the underlying structural principles for their shared function, i.e. non-specific binding of hydrophobic ligands such as fatty acids, are intriguingly similar. The first three α -helices from each sub-domain of HSA correspond approximately to the first three α -helices, H1-H3, of plant nsLTPs. The fourth long α -helix at the C terminus of the HSA sub-domain, however, lies on the same side as the N terminus, whereas helix H4 and the winding C-terminal loop in plant nsLTPs are positioned on the opposite side from the N terminus. Notwithstanding this difference, the hydrophobic binding pockets are formed between α -helices in both HSA and plant nsLTPs (Figure 6). The five myristate binding sites in HSA, though not identical with each other, share some features in common. The methylene tail of the fatty acid is accommodated within a deep hydrophobic cavity, while the carboxylate moiety interacts with two or three, basic (Arg or Lys) or polar (Tyr or Ser) residues. The orientations of two myristate moieties (Myr1 and Myr5) are inverted. In addition, no myristate molecule is bound to sub-domain IIB, because the hydrophobic tunnel is severely constricted at the center by aromatic side-chains, and the end of the tunnel corresponding to the myristate carboxylate binding site is occluded by a short helix.²⁷ A similar binding mode of phosphatidylcholine was found in human bactericidal/permeability-increasing protein (BPI; PDB code: 1bp1), a member of the lipopolysaccharide-binding and lipid-transport protein family. In this BPI-phosphatidylcholine complex, both acyl chains of phosphatidylcholine are buried inside the hydrophobic cavity and the head group is exposed to the

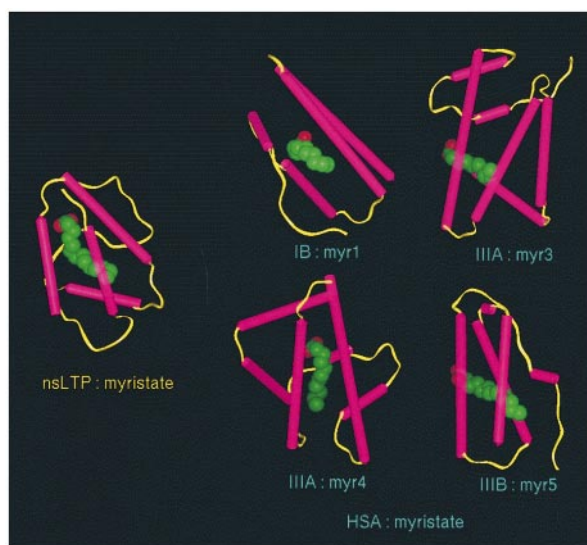


Figure 6. Comparisons of nsLTP:myristate with human serum albumin (HSA) in complex with myristate moieties. Insight II v97.5 (Molecular Simulations, Inc.) was used for the display. The three domains of HSA bind five myristate moieties; four are shown here, myr1, myr3, myr4, and myr5.

solvent, interacting with nearby Arg432 and Tyr455.²⁸ The phosphorus oxygen (O2P) atom of the head group is hydrogen bonded with the NH2 group of Arg432 as well as the OH group of Tyr455 in the complex. A similar nsLTP interaction with an Arg46 outside the binding cavity occurs in the nsLTP:oleate complex reported here.

Biological implications of multiple binding modes of caprate and oleate

The two different conformations of oleate exhibit reasonable hydrophobic interactions as well as hydrogen bonding of the carboxyl head groups, implying that both conformations are bound equally well and have good transfer activity in solution. It also suggests that both oleate conformations have a binding affinity similar to other fatty acids. Like oleate, the two alternate conformations of caprate have similar binding affinities to each other. However, fewer hydrophobic interactions and the absence of a hydrogen bond between the carboxyl head group of caprate and the protein suggest that both alternate conformations have a lower affinity than other fatty acids for maize nsLTP.

The observation of multiple binding modes is rare in most enzyme-ligand complexes. Whereas in the case of enzyme-substrate interactions binding geometry must be precise in order for catalysis to occur, nsLTPs are not constrained by catalytic requirements. Their biological role is to transfer lipids. Apparently multiple binding modes are one

Table 3a. Crystallization conditions and unit cell parameters

Ligand	Crystallization condition in reservoir solution	Crystal size (mm)	Unit cell parameter ($a, b, c, \text{Å}; \alpha, \beta, \gamma, ^\circ$)	Space group
None	100 mM Hepes & 1.2 M trisodium citrate (pH 8.4)	0.7×0.4×0.3	$a=24.46, b=49.97, c=69.99,$ $\alpha=\beta=\gamma=90$	$P2_12_12_1$
Capric acid C10:0	3.3 M Na formate & 10% (v/v) glycerol	0.2×0.15×0.1	$a=24.75, b=49.87, c=69.42,$ $\alpha=\beta=\gamma=90$	$P2_12_12_1$
Lauric acid C12:0	4.2 M Na formate & 0.2 M potassium cyanide	0.1×0.2×0.3	$a=24.82, b=49.68, c=69.60,$ $\alpha=\beta=\gamma=90$	$P2_12_12_1$
Myristic acid C14:0	4.2 M Na formate	0.1×0.25×0.3	$a=24.75, b=49.47, c=69.62,$ $\alpha=\beta=\gamma=90$	$P2_12_12_1$
Palmitic acid C16:0	3.4 M Na formate	0.2×0.25×0.8	$a=24.80, b=49.60, c=70.10,$ $\alpha=\beta=\gamma=90$	$P2_12_12_1$
Palmitoleic acid C16:1, 9	4.5 M Na formate & 0.1 M lithium sulfate	0.1×0.2×0.3	$a=24.79, b=49.79, c=69.45,$ $\alpha=\beta=\gamma=90$	$P2_12_12_1$
Stearic acid C18:0	5.0 M Na formate	0.3×0.2×0.1	$a=24.81, b=50.00, c=69.53,$ $\alpha=\beta=\gamma=90$	$P2_12_12_1$
Oleic acid C18:1, 9	3.6–4.8 M Na formate	0.3×0.2×0.3	$a=24.68, b=49.72, c=69.20,$ $\alpha=\beta=\gamma=90$ (at synchrotron radiation)	$P2_12_12_1$
Linolenic acid C18:3, 9,12,15	4.4 M Na formate & 0.1 M benzene sulfonic acid	0.15×0.2×0.3	$a=25.04, b=50.36, c=69.47,$ $\alpha=\beta=\gamma=90$	$P2_12_12_1$
Ricinoleic acid C18:1, 9, 12-OH	5.0 M Na formate	0.2×0.2×0.35	$a=24.81, b=49.88, c=69.41,$ $\alpha=\beta=\gamma=90$	$P2_12_12_1$

Table 3b. Data collection statistics

	Resolution (Å)	No. of total observations	No. of unique reflections	R_{sym} (%)	Completeness (%)
Capric acid C10:0	1.76	23,393	8379	2.9	89.2
Lauric acid C12:0	1.76	23,095	8570	4.4	91.4
Myristic acid C14:0	1.76	21,620	8516	4.2	92.0
Palmitoleic acid C16:1, 9	1.69	22,830	9248	2.6	92.2
Stearic acid C18:0	1.66	24,039	9510	4.0	90.4
Oleic acid C18:1, 9	1.30	93,324	18,062	5.7	75.7
Linolenic acid C18:3, 9,12,15	1.80	18,547	6996	4.7	92.6
Ricinoleic acid C18:1, 9, 12-OH	1.65	21,681	8002	2.9	82.7

means by which nsLTPs have evolved to bind and transport lipids.

Materials and Methods

Protein purification and crystallization

The procedures for the purification and crystallization of nsLTP from maize seedlings have been described.²⁹ The crystallization of maize nsLTP, both uncomplexed and in complex with various ligands, was performed essentially as above, except that each ligand was present in the hanging drop in various molar ratios (1–1.5:1), sodium formate was used as the precipitant, and additives were included for some ligands. The bound ligands are C10 to C18 saturated or unsaturated fatty acids. The optimum crystallization condition had to be fine-tuned for each of the complexes (Table 3(a)) because their solubility properties showed some variation. This suggests that the surface characteristics of the complexes are not exactly identical.

The complex crystals were grown from sodium formate. Despite much effort, the complex crystals could not be grown using the original citrate conditions reported for uncomplexed crystals.²⁹ The optimum crystallization conditions varied from one ligand to another. The concentration of sodium formate ranged between

3.3 M and 5.0 M for complexes with different ligands. The crystals of complexed nsLTP were isomorphous with the uncomplexed crystal with similar unit cell parameters in the space group $P2_12_12_1$. The crystallization conditions and unit cell parameters are summarized in Table 3(a).

Data collection

Most sets of X-ray data were collected at 20 °C on a FAST TV-area detector (Enraf-Nonius) using the MADNES software³⁰ with monochromatic CuK α X-rays from a rotating anode generator (Rigaku RU-200). The reflection intensities were obtained by a profile-fitting procedure³¹ and the data were scaled by a Fourier scaling program.³² The synchrotron data from nsLTP (uncomplexed and oleate complex) were collected at 14 °C using a Weissenberg camera for macromolecular crystallography at the BL-6A2 experimental station of the Photon Factory, Tsukuba, Japan.³³ The wavelength of the X-rays used was 1.000 Å and a 0.1 mm collimator was used. A Fuji image plate (type BAIII, 20 cm × 40 cm) was placed at a distance of 273 mm from the crystal. The oscillation range per image plate was 5.0° with a speed of 2.0°/second and a coupling constant of 1.0°/mm for the a -axis rotation, and 4.5° with a speed of 2.0°/second and a coupling constant of

Table 4a. Refinement statistics using the data from the FAST area detector (in house)

Ligand	Resolution range (Å)	No. of refls	No. of protein atoms	No. of solvent molecules		No. of ligand atoms	<i>R</i> -factor (<i>R</i> _{free}) (%)	r.m.s. deviation	
				water	formate			bond length (Å)	bond angle (°)
Capric acid C10:0	8.0-1.8	7436	625	59	1	12	21.4 (24.1)	0.016	1.77
Lauric acid C12:0	8.0-1.8	7638	625	63	2	14	19.5 (21.1)	0.014	1.63
Myristic acid C14:0	8.0-1.8	7670	625	93	1	16	19.1 (19.7)	0.015	1.70
Palmitic acid C16:0	8.0-1.78	7314	625	68	1	18	17.1 (17.7)	0.013	1.72
Palmitoleic acid C16:1, 9	8.0-1.8	8241	625	54	1	18	20.0 (23.6)	0.013	1.60
Stearic acid C18:0	8.0-1.8	7961	625	70	3	20	20.0 (20.8)	0.014	1.73
Linolenic acid C18:3, 9,12,15	8.0-1.9	6390	625	68	2	20	20.7 (27.4)	0.015	1.70
Ricinoleic acid C18:1, 9, 12-OH	8.0-1.9	6686	625	73	1	20	20.5 (27.4)	0.014	1.60

Table 4b. Refinement statistics using the data from synchrotron radiation at the Photon Factory

Ligand	Resolution range (Å)	No. of refls	No. of protein atoms	No. of solvent molecules			<i>R</i> -factor (<i>R</i> _{free}) (%)	r.m.s. deviation	
				water	formate	No. of ligand atoms		bond length (Å)	bond angle (°)
Oleic acid C18:1, 9	8.0-1.3	13,391	625	121	3	22	13.5 (18.8)	0.009	2.20

1.8°/mm for the *c*-axis rotation. An overlap of 0.5° was allowed between two contiguous image plates. The diffraction patterns recorded on the image plates were digitized by a Fuji BA100 scanner. The raw data were processed using the program WEIS.³⁴ Table 3(b) gives a summary of the data collection and data-reduction parameters.

Structure solution, refinement, and analysis

Each model of the complexed protein was refined independently of the others in order to avoid bias from the previous models. The model of the uncomplexed maize nsLTP (PDB code: 1mzl) was subject to rigid-body refinement followed by positional refinement, simulated annealing refinement, and *B*-factor refinement using the program X-PLOR.³⁵ When the *R*-factor reached below 25%, both ($2F_o - F_c$) and ($F_o - F_c$) omit maps were calculated to model the bound fatty acids in the hydrophobic cavity. The graphics programs CHAIN,³⁶ running on a Silicon Graphics Indigo2 Extreme workstation, and O,³⁷ running on a Dec Alpha CompaQ, were used. After fitting each ligand model into the electron density, the complexed structure was further refined using X-PLOR. For the 1.3 Å synchrotron data of the nsLTP:oleate complex, an anisotropic temperature refinement (Table 4(b)) was carried out using SHELXL-97.³⁸ All the models have been refined against X-ray diffraction data extending to either 1.8-1.9 Å or 1.3 Å to reasonable *R*-factors with good stereochemistry. All the models have favorable backbone conformational angles; all non-glycine residues are in favorable regions of the Ramachandran plot as indicated by PROCHECK.³⁹ The refinement statistics are listed in Table 4. The van der Waals volume of the hydrophobic cavity was calculated using VOIDOO²⁶, after removing the bound ligands from the models of complexed structures. Cavity volumes for ten different orientations were averaged. For structure comparisons,

solution structures determined by NMR were averaged by the program MOLMOL.⁴⁰

Protein Data Bank accession numbers

Coordinates for the refined models and structure factors have been deposited with the Protein Data Bank (accession codes: 1fk0 for nsLTP:caprate, 1fk1 for nsLTP:laurate, 1fk2 for nsLTP:myristate, 1fk3 for nsLTP:palmitoleate, 1fk4 for nsLTP:stearate, 1fk5 for nsLTP:oleate, 1fk6 for nsLTP:linolenate, and 1fk7 for nsLTP:ricinoleate).

Acknowledgments

We thank Professor N. Sakabe and his staff for assistance with synchrotron X-ray data collection at beamline BL-6A of the Photon Factory, Japan. We are indebted to Professor Richard Dickerson for supporting the completion of our project at UCLA. This work was supported by the Center for Molecular Catalysis, Seoul National University. S.W.S. is supported by the BK 21 Program. G.W.H. was supported by a Postdoctoral Fellowship from the Korean Ministry of Education.

References

- Rueckert, D. G. & Schmidt, K. (1990). Lipid transfer proteins. *Chem. Phys. Lipids*, **56**, 1-20.
- Breu, V., Guerbet, F., Kader, J. C., Kannangara, C. G., Svensson, B. & Wettstein-Knowles, P. (1989). A 10 kDa barley basic protein transfers phosphatidylcholine from liposomes to mitochondria. *Carlsberg. Res. Commun.* **54**, 81-84.

3. Sterk, P., Booij, H., Schellekens, G. A., Van Kammen, A. & De Vries, S. C. (1991). Cell specific expression of the carrot EP2 lipid-transfer protein gene. *Plant Cell*, **3**, 907-921.
4. Meijer, E. A., De Vries, S. C., Sterk, P., Gadella, D. W., Wirtz, K. W. A. & Hendriks, T. (1993). Characterization of the non-specific lipid-transfer protein EP2 from carrot (*Daucus carota* L.). *Mol. Cell. Biochem.* **123**, 159-166.
5. Hollenbach, B., Schreiber, L., Hartung, W. & Dietz, K. J. (1997). Cadmium leads to stimulated expression of the lipid-transfer protein genes in barley: implications for the involvement of lipid-transfer proteins in wax assembly. *Planta*, **203**, 9-19.
6. Terras, F. R. G., Goderis, I. J., Van Leuvren, F., Vanderleyden, J., Cammue, B. P. A. & Broekaert, W. F. (1992). *In vitro* antifungal activity of a radish (*Raphanus sativus* L.) seed protein homologous to nonspecific lipid-transfer proteins. *Plant Physiol.* **100**, 1055-1058.
7. Molina, A. & Garcia-Olmedo, F. (1993). Developmental and pathogen-induced expression of three barley genes encoding lipid-transfer proteins. *Plant J.* **4**, 983-991.
8. Molina, A., Segura, A. & Garcia-Olmedo, F. (1993). Lipid transfer proteins (nsLTPs) from barley and maize leaves are potent inhibitors of bacterial and fungal plant pathogens. *FEBS Letters*, **316**, 119-122.
9. Tsuboi, S., Osafune, T., Nishimura, M. & Yamada, M. (1992). Nonspecific lipid-transfer protein in castor bean cotyledon cells: subcellular localization and a possible role in lipid metabolism. *J. Biochem.* **111**, 500-508.
10. Arondel, V., Vergnolle, C., Tchang, F. & Kadar, J. C. (1990). Bifunctional lipid-transfer: fatty acid-binding proteins in plants. *Mol. Cell. Biochim.* **98**, 49-56.
11. Østergaard, J., Vergnolle, C., Schoentgen, F. & Kader, J. (1993). Acyl-binding/lipid-transfer proteins from rape seedlings, a novel category of proteins interacting with lipids. *Biochim. Biophys. Acta*, **1170**, 109-117.
12. Tchang, F., This, P., Stiefel, V., Arondel, V., Morch, M., Pages, M., Puigdomenech, P., Grellet, F., Delseny, M., Bouillon, P., Huet, J., Guerbet, F., Beauvais-Cante, F., Duranton, H., Pernollet, J. & Kader, J. C. (1988). Phospholipid-transfer protein: full-length cDNA and amino acid sequence in maize. *J. Biol. Chem.* **263**, 16849-16855.
13. Simorre, J.-P., Caille, A., Marion, D., Marion, D. & Ptak, M. (1991). Two- and three-dimensional ¹H NMR studies of a wheat phospholipid-transfer protein: sequential resonance assignments and secondary structure. *Biochemistry*, **30**, 11600-11608.
14. Gincel, E., Simorre, J. P., Caille, A., Marion, D., Ptak, M. & Vovelle, F. (1994). Three-dimensional structure in solution of a wheat lipid-transfer protein from multidimensional ¹H-NMR data. A new folding for lipid carriers. *Eur. J. Biochem.* **226**, 413-422.
15. Shin, D. H., Lee, J. Y., Hwang, K. Y., Kim, K. K. & Suh, S. W. (1995). High-resolution crystal structure of the non-specific lipid-transfer protein from maize seedlings. *Structure*, **3**, 189-199.
16. Lee, J. Y., Min, K., Cha, H., Shin, D. H., Hwang, K. Y. & Suh, S. W. (1998). Rice non-specific lipid-transfer protein: the 1.6 Å crystal structure in the unliganded state reveals a small hydrophobic cavity. *J. Mol. Biol.* **276**, 437-448.
17. Gomar, J., Petit, M. C., Sodano, P., Sy, D., Marion, D., Kader, J. C., Vovelle, F. & Ptak, M. (1996). Solution structure and lipid binding of a nonspecific lipid-transfer protein extracted from maize seeds. *Protein Sci.* **5**, 565-577.
18. Lerche, M. H., Kragelund, B. B., Bech, L. M. & Poulsen, F. M. (1997). Barley lipid-transfer protein complexed with palmitoyl CoA: the structure reveals a hydrophobic binding site that can expand to fit both large and small lipid-like ligands. *Structure*, **5**, 291-306.
19. Poznanski, J., Sodano, P., Suh, S. W., Lee, J. Y., Ptak, M. & Vovelle, F. (1999). Solution structure of a lipid-transfer protein extracted from rice seeds. Comparison with homologous proteins. *Eur. J. Biochem.* **259**, 692-708.
20. Baud, F., Pebay-Peyroula, E., Cohen-Addad, C., Odani, S. & Lehmann, M. S. (1993). Crystal structure of hydrophobic protein from soybean: a member of a new cysteine-rich family. *J. Mol. Biol.* **231**, 877-887.
21. Murzin, A. G. (1994). New protein folds. *Curr. Opin. Struct. Biol.* **4**, 441-449.
22. Charvolin, D., Douliez, J.-P., Marion, D., Cohen-Addad, C. & Pebay-Peyroula, E. (1999). The crystal structure of a wheat nonspecific lipid-transfer protein (ns-LTP1) complexed with two molecules of phospholipid at 2.1 Å resolution. *Eur. J. Biochem.* **264**, 562-568.
23. Lerche, M. H. & Poulsen, F. M. (1998). Solution structure of barley lipid-transfer protein complexed with palmitate. Two different binding modes of palmitate in the homologous maize and barley nonspecific lipid-transfer proteins. *Protein Sci.* **7**, 2490-2498.
24. Sodano, P., Caille, A., Sy, D., de Person, G., Marion, D. & Ptak, M. (1997). ¹H NMR and fluorescence studies of the complexation of DMPG by wheat non-specific lipid-transfer protein. Global fold of the complex. *FEBS Letters*, **416**, 130-134.
25. Tassin-Moindrot, S., Caille, A., Douliez, J.-P. & Vovelle, F. (2000). The wide binding properties of a wheat nonspecific lipid-transfer protein. Solution structure of a complex with prostaglandin B₂. *Eur. J. Biochem.* **267**, 1117-1124.
26. Kleywegt, G. J. & Jones, T. A. (1994). Detection, delineation, measurement and display of cavities in macromolecular structures. *Acta Crystallog. sect. D*, **50**, 178-185.
27. Curry, S., Mandelkow, H., Brick, P. & Franks, N. (1998). Crystal structure of human serum albumin complexed with fatty acid reveals an asymmetric distribution of binding sites. *Nature Struct. Biol.* **5**, 827-835.
28. Beamer, L. J., Carroll, S. F. & Eisenberg, D. (1997). Crystal structure of human BPI and two bound phospholipids at 2.4 Å resolution. *Science*, **276**, 1861-1864.
29. Shin, D. H., Hwang, K. Y., Kim, K. K., Kim, S., Sweet, R. M. & Suh, S. W. (1994). Crystallization and preliminary X-ray crystallographic analysis of phospholipid-transfer protein from maize seedlings. *Proteins: Struct. Funct. Genet.* **19**, 80-83.
30. Messerschmidt, A. & Pflugrath, J. W. (1987). Crystal orientation and X-ray pattern prediction routines for area-detector diffractometer systems in macromolecular crystallography. *J. Appl. Crystallog.* **20**, 306-315.
31. Kabsch, W. (1988). Evaluation of single-crystal X-ray diffraction data from a position-sensitive detector. *J. Appl. Crystallog.* **21**, 916-924.
32. Weissman, L. (1982). Strategies for extracting isomorphous and anomalous signals. In *Computational*

- Crystallography* (Sayre, D., ed.), pp. 56-63, Oxford University Press (Clarendon), Oxford.
33. Sakabe, N. (1991). X-ray diffraction data collection system for modern protein crystallography with a Weissenberg camera and an imaging plate using synchrotron radiation. *Nucl. Instrum. Methods A*, **303**, 448-463.
 34. Higashi, T. (1989). The processing of diffraction data taken on a screenless Weissenberg camera for macromolecular crystallography. *J. Appl. Crystallog.* **22**, 9-18.
 35. Brünger, A. T. (1992). *X-PLOR (version 3.1): A system for X-ray Crystallography and NMR*, Yale University Press, New Haven, CT.
 36. Sack, J. S. (1988). CHAIN: a crystallographic modeling program. *J. Mol. Graph.* **6**, 244-245.
 37. Jones, T. A., Zou, J. Y., Cowan, S. W. & Kjeldgaard, M. (1991). Improved methods for building protein models in electron density maps and the location of errors in these models. *Acta Crystallog. sect. A*, **47**, 110-119.
 38. Sheldrick, G. M. & Schneider, T. R. (1997). SHELXL: high resolution refinement. *Methods Enzymol.* **277**, 319-343.
 39. Laskowski, R. A., MacArthur, M. W., Moss, D. S. & Thornton, J. M. (1993). PROCHECK: a program to check the stereochemical quality of protein structures. *J. Appl. Crystallog.* **26**, 283-291.
 40. Koradi, R., Billeter, M. & Wuthrich, K. (1996). MOLMOL: a program for display and analysis of macromolecular structures. *J. Mol. Graph.* **14**, 51-55.
 41. Kraulis, P. J. (1991). MOLSCRIPT: a program to produce both detailed and schematic plots of protein structures. *J. Appl. Crystallog.* **24**, 946-950.
 42. Nicholls, A., Bharadwaj, R. & Honig, B. (1993). GRASP: graphical representation and analysis of surface properties. *Biophys. J.* **64**, 166-170.
 43. Connolly, M. L. (1983). Solvent-accessible surfaces of proteins and nucleic acids. *Science*, **221**, 709-713.
 44. Evans, S. V. (1993). SETOR-hardware-lighted 3 dimensional solid model representations of macromolecules. *J. Mol. Graph.* **11**, 134-138.

Edited by D. Rees

(Received 3 November 2000; received in revised form 8 February 2001; accepted 12 February 2001)